Experiments in Fluids (2020) 61:77
https://doi.org/10.1007/s00348-020-2909-9

RESEARCH ARTICLE

Characterization of tracers for two-color laser-induced fluorescence liquid-phase temperature imaging in sprays

Markus Michael Prenting[1] · Muhammad Imran Bin Dzulfida[1] · Thomas Dreier[1] · Christof Schulz[1]

Received: 14 October 2019 / Revised: 27 December 2019 / Accepted: 31 January 2020

Abstract

The variation of the fluorescence spectral signature of tracer solutions with temperature enables temperature imaging measurements in liquids and sprays by simultaneously recording and rationing the fluorescence intensity detected in two separate wavelength channels. In this work, we recorded fluorescence spectra of ethanol-based solutions of nine laser dyes used as tracers (PTP, stilbene 1, coumarin 152, coumarin 153, rhodamine B, rhodamine 101, pyrromethene 597, DCM, and pyridine 1) after excitation at either 266, 355, or 532 nm (depending on the dye) for temperatures between 298 and 348 K (close to the boiling point of the solvent), and for concentrations (depending on dye) around 10 mg/l (i.e., ~ 10^{-5} mol/l). The influence of signal self-absorption was investigated for the tracers best suited for thermometry, rhodamine B and coumarin 152, where the latter is almost unaffected due to its large Stokes shift. In thin-film (100 µm) cells, possible concentration effects on the fluorescence spectrum were investigated in the absence of signal self-absorption in the 0.1–10 and 0.5–50 mg/l range for rhodamine B and coumarin 152, respectively. Sensitivities of the two-color intensity ratios were determined for two selected color detection channels for each tracer characterized by their center wavelength and spectral half width and conditioned on averaged intensities of larger than 10% of the spectral peak of their respective fluorescence spectrum. The use of coumarin 152 that showed the overall best spectroscopic properties was demonstrated for temperature imaging in a burning ethanol spray.

✉ Markus Michael Prenting
markus.prenting@uni-due.de

[1] IVG, Institute for Combustion and Gas Dynamics - Reactive Fluids, and CENIDE, Center for Nanointegration Duisburg-Essen, University of Duisburg-Essen, Duisburg, Germany

Published online: 21 February 2020

Graphic abstract

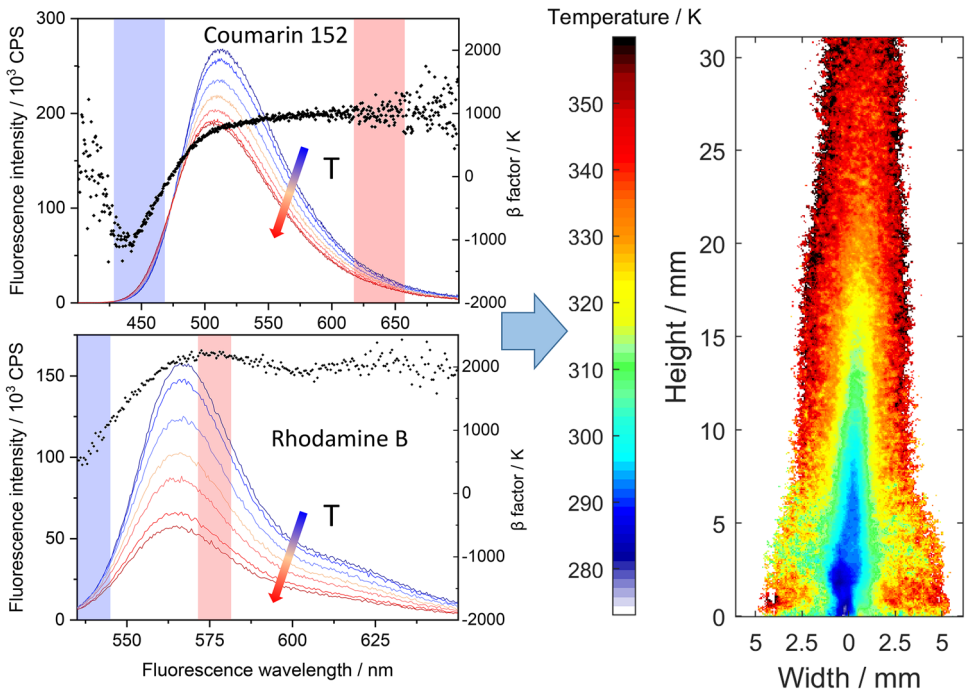

1 Introduction

The experimental visualization and quantitative measurement of sprays is an active and challenging field of research. These efforts aim at understanding the involved transport phenomena and fluid mechanics during liquid disintegration, droplet breakup, droplet evaporation and vapor mixing with the surrounding gas phase, e.g., in the context of improvement of combustion processes. One important quantity of interest is the droplet temperature that is affected by heat transfer with the surrounding (potentially reacting) gas and evaporative cooling and thus affects evaporation. The droplet temperature is of specific interest in dynamic processes that can lead to droplet superheating and eventually to droplet explosion, especially in case the liquid contains components with different boiling points (Rosebrock et al. 2016; Wang et al. 2005). It can also be important in processes where reactions such as pyrolysis or precipitation can occur inside the droplet above a specific temperature (Angel et al. 2019). Therefore, in situ measurements of the liquid-phase temperature in sprays—if possible with high temporal and spatial resolution—are highly desired. A variety of optical imaging methods has been explored and applied for spray temperature characterization, and only a few examples will be given in this introduction. The interested reader is referred to reviews and textbooks, also covering other measurement techniques for spray characterization (Lefebvre and McDonell 2017; Tropea et al. 2007).

Various physical effects can be used to measure the liquid-phase temperature. Temperature-induced changes in molecular interaction affect absorption and Raman spectra. For temperature measurements in, e.g., thin water films, near-infrared absorption has been applied for temperature measurements (Yang et al. 2011). Due to the line-of-sight integration in absorption measurements, the transfer to sprays is not straight forward. Recording Raman spectra (Raffius et al. 2017) and relating spectral features to calibrated ones from a data base of known conditions has been done for ethanol (Muller et al. 2000) and water (Heinisch et al. 2009; Walrafen et al. 1998) sprays. The drawback of Raman scattering in two-phase flows is interference from the much stronger Rayleigh/Mie scattering and its low signal strength, therefore being limited to point or one-dimensional imaging measurements. In addition, the appearance of morphology-dependent resonances within larger droplets make quantitative measurements difficult (Schaschek et al. 1993; Snow et al. 1985).

Exploiting the temperature dependence of the refractive index, rainbow refractometry has been used for temperature measurements in single droplets (Roth et al. 1991). Here, the wavelength-dependent refraction generates a “rainbow” by illuminating the droplet with broadband light. The angular

position of the rainbow depends on the refractive index of the liquid and thus on temperature. In case the refractive index is not constant throughout the droplet volume, e.g., because of local variations in temperature or composition, the evaluation needs to rely on a thorough model understanding of heat transfer and conduction (Horn and Chigier 2002). Additionally, only single droplets can be investigated to not corrupt a quantitative post processing of the rainbow signatures through secondary scattering and refraction.

Local measurements that can be expanded to imaging of the desired quantity in cross-sectional planes through the spray upon illumination with a laser light sheet are often based on laser-induced fluorescence (LIF)—that in contrast to Raman scattering provides much stronger signal and due to its spectral shift, easier separation from elastically scattered light. While secondary scattering of laser and signal light can blur the spatial resolution, this issue can be overcome by employing structured illumination techniques (Berrocal et al. 2008; Mishra et al. 2016).

For LIF measurements, especially when aiming at thermometry, usually fluorescent tracers with well-defined spectroscopic properties are added to the liquid of interest. For droplet and spray visualization in evaporating sprays, it is important that the fluorescing component co-evaporates with the spray. For hydrocarbon-based liquids, species like aromatics and ketones are used for this purpose (Schulz and Sick 2005), while for water-based liquids, species like ethyl acetoacetate (Greszik et al. 2011) were applied. However, in a rapidly evaporating spray, the evaporated tracers can cause a significant LIF signal contribution from the gas phase. Therefore, sometimes co-evaporating systems were chosen that form an exciplex in the liquid phase, e.g., from a laser-excited so-called monomer (e.g., fluorine-substituted benzene and/or toluene) and a quencher (e.g., tertiary amines), that generates emission that is strongly red-shifted compared to the fluorescence of the individual constituents and thus can be discriminated against signal contribution from the gas phase (Duwel et al. 2009; Melton 1993; Wieske et al. 2006). The limited thermal stability of the exciplex leads to a variation of the emission spectra with temperature and the relative signal from two selected emission bands can be exploited for thermometry after calibration at known temperatures. A severe drawback of this method is that due to efficient fluorescence quenching by oxygen, measurements can only be performed in oxygen-free environments.

For temperature measurements, co-evaporation of tracer and liquid is not required because the absolute signal intensity (i.e., the local tracer concentration) cancels through ratiometric analysis of the signal recorded in two separate spectral regions. Therefore, it is often better to use non-evaporating tracers such as laser dyes and take advantage of their very high fluorescence quantum yield (enabling measurements with very small tracer concentration typically in the 10 mg/l, i.e., 3×10^{-5} mol/l range) and their temperature-dependent spectral emission features. At the same time, signal contributions from the gas phase are not expected alleviating the above-mentioned problem of separating gas-phase and liquid-phase information. The use of laser dyes as temperature tracers in liquids has been pioneered by Murray and Melton (1985) and Lavieille et al. (2000) and has been applied by other research groups (Chaze et al. 2016; Mishra et al. 2016). Because of the broadband absorption characteristics of the laser dyes, fluorescence can be excited conveniently with the harmonics of Nd:YAG laser radiation. Temperature measurements are accomplished by forming intensity ratios of two detection channels recording separate wavelength ranges of the fluorescence spectrum with different temperature dependences.

Rhodamine B has been used extensively for temperature imaging (Lavieille et al. 2001). With 514 nm excitation and fluorescence detection in two spectral bands [channel 1: bandpass filter (center wavelength: 530 nm, FWHM: 10 nm); channel 2: $\lambda > 590$ nm] a temperature measurement precision of 1 K was achieved with single-color fluorescence detection of single ethanol droplets within a droplet chain, with uncertainties mainly caused by droplet evaporation which causes temporal changes in dye concentration. The same group also applied two-color LIF thermometry with rhodamine B (Lavieille et al. 2001).

For the rhodamine dyes utilized in the previous work, absorption and fluorescence spectra partially overlap, which can cause reabsorption and concentration-dependent variations of the recorded fluorescence intensities when one of the detection bands is located in this overlap region. To circumvent this problem, either a second dye whose fluorescence is well spectrally separated from the first one can be added to the solvent (Copetta and Rogers 1998), or a three-color detection technique (Lavieille et al. 2004) can be applied. Tracer species with a larger Stokes shift—as introduced in our work with coumarin dyes—are more appropriate for such applications and circumvent the signal re-absorption problem without adding a third detection channel.

In the present work, we investigated the potential of various dyes for thermometry in ethanol by recording their temperature-dependent fluorescence spectra after excitation at standard ultraviolet and visible wavelengths corresponding to Nd:YAG laser harmonics. We compare their respective fractional temperature sensitivities (i.e., the difference in the "temperature sensitivity factors β") in the two-color intensity ratio method, and in particular contrast rhodamine B—a well characterized dye from literature—with coumarin 152, which exhibits a significantly larger Stokes shift making it a promising candidate for measurements in situations where self-absorption is an issue. For a fixed spectral half-width, the temperature sensitivity of the ratio method is also evaluated as a function of the spectral separation of the two

detection windows in the two-color LIF thermometry. For coumarin 152 we demonstrate temporally averaged temperature imaging of an ethanol spray flame.

2 Principle of two-color LIF thermometry

The principle of two-color LIF thermometry using tracers with broadband fluorescence spectra is based on their temperature-dependent fluorescence spectra. The derivation of the relevant LIF intensity equations is presented in the literature, e.g., by Ref. (Deprédurand et al. 2008; Lavieille et al. 2001) and will be only briefly described here. The temperature dependence of the LIF intensity can generally be well approximated by an exponential relation $I_{\mathrm{LIF}}(T) \sim \exp(\beta(\lambda)/T)$ (Lavieille et al. 2001), where $\beta(\lambda)$ is the so-called temperature-sensitivity factor. This factor describes the extent of the variation in fluorescence intensity of the respective tracer as a function of temperature at a given wavelength. Increasing intensity (with increasing temperature) results in negative values, decreasing intensity in positive β values. Large absolute values of β (either positive or negative) are required for sensitive single-line thermometry. For two-line thermometry, the absolute value and its sign is meaningless (other that it indicates either a gain or a loss in signal-to-noise ratio with increasing temperature). The relevant value here is the difference in β for the two spectral bands chosen for the ratiometric analysis. Upon laser excitation at a fixed wavelength within the absorption spectrum, the resulting signal is

$$I_{\mathrm{LIF}} = nV\sigma I_0 \exp\left(\beta(\lambda)/T\right)\eta, \tag{1}$$

with the tracer concentration n, the probe volume V, the absorption cross-section at the laser wavelength σ, the laser fluence I_0, and the detection efficiency η.

As will be seen in Sect. 4.1 and the supplemental material, β of all investigated tracers varies with fluorescence wavelength. Therefore, temperature can be inferred from measured fluorescence intensities by placing appropriate spectral filters with selected transmission bands and center wavelengths [illustrated in Fig. 1 with the (λ_1, λ_2) pair, respectively] in front of the detectors and forming the respective signal intensity ratios (Lavieille et al. 2001).

$$R_{\mathrm{LIF}}(T) = \frac{\eta_1}{\eta_2}\exp\left(\left(\beta_1 - \beta_2\right)/T\right). \tag{2}$$

This ratio already cancels several unknown quantities in Eq. (1). When the same ratio is formed at a known reference temperature, only parameters characteristic of the tracer fluorescence remain and provide a logarithmic intensity ratio linear in the difference of the inverse temperature values (Lavieille et al. 2001):

$$\ln\left(\frac{R_{\mathrm{LIF}}(T)}{R_{\mathrm{LIF}}(T_0)}\right) = \left(\beta_1 - \beta_2\right)\left(\frac{1}{T} - \frac{1}{T_0}\right). \tag{3}$$

Therefore, the slope difference $\Delta\beta_{12} = \beta_1 - \beta_2$ of the temperature-sensitivity factors between both detection channels is a measure for the temperature sensitivity of the two-color ratio LIF thermometry. Knowing the ratio at a given temperature T_0, the temperature of the liquid can be derived from

$$T = \Delta\beta_{12}T_0 \Big/ \left(\ln\left(\frac{R_{\mathrm{LIF}}(T)}{R_{\mathrm{LIF}}(T_0)}\right) + \left(\beta_1 - \beta_2\right)\right). \tag{4}$$

With tracer concentrations n in the 10^{-5} mol/l range in our experiments, self-quenching is not important, because according to the relation derived in Lavieille et al. (2001) (Sect. 3.2.2), the threshold value of $n < 0.01\ C^*$ (with a critical concentration C^* for self-quenching of approx. 0.6 mol/l for rhodamine B) is not violated.

3 Experimental details

3.1 Measurement of absorption/fluorescence spectra

Absorption and fluorescence spectra of various tracers in ethanol were recorded with analytical instruments—an absorption spectrometer (Varian Inc., Mod. Cary 400) and a fluorescence spectrometer (Horiba, Fluorolog-3 Model FL3-22). The latter consists of an excitation monochromator, equipped with a xenon lamp for sample excitation (1 nm bandwidth) and an emission monochromator (1 nm bandwidth) for scanned spectra recording with a photomultiplier tube. The choice of excitation wavelength for each tracer in this work is listed in Table 1, and was determined by their respective absorption spectra and driven by the need in standard applications, which utilize easily accessible wavelengths of harmonics of a Nd:YAG laser.

The tracer solutions were prepared in a two-step dilution process by weighing the solid powder and dissolving them in known volumes of ethanol resulting in solutions with concentrations of 10 mg/l that are then further diluted to the desired concentration level. For the measurements the solution was filled into an optical quartz cell (Hellma cuvette 111-QS, 10×10 mm^2) and placed into a temperature-controlled stainless-steel container. The temperature of the ethanol/tracer solution was measured with a thermocouple (type K) directly placed into the liquid. The container was then placed into the spectrometer sample compartment where the fluorescence radiation is recorded at 90° relative to the excitation beam and recorded with an increment of 0.5 nm with an integration

Table 1 List of tracers investigated in this work

Laser dye	Concentration /(mg/l)	Concentration /(mol/l)	Excitation wavelength /nm	Molar mass /(g/mol)
Coumarin 152	0.5–50	1.9×10^{-6}–1.9×10^{-4}	266/355	257.21
Coumarin 153	2.5–10	8×10^{-6}–1.3×10^{-5}	266	309.28
DCM	10	3.3×10^{-5}	266	303.37
Pyridine 1	10	2.6×10^{-5}	532	378.85
Pyrromethene 597	1–10	2.7×10^{-6}–2.7×10^{-5}	532	374.32
PTP (*p*-Terphenyl)	10	4.3×10^{-5}	266	230.31
Rhodamine 101	6.4	1×10^{-5}	532	591.06
Rhodamine B	0.1–10	2.1×10^{-7}–2.1×10^{-5}	532	479.02
Stilbene 3	10	1.8×10^{-5}	355	562.56

The tracers were dissolved in ethanol

time of 0.1 s. Depending on the fluorescence intensity per temperature step, three to five spectra were averaged to improve the signal-to-noise ratio.

Table 1 lists the tracers for which the temperature-dependent fluorescence spectra were measured after excitation at the listed wavelengths. The spectra were measured within a temperature range from room temperature to 75 °C—close to the boiling point of ethanol. The tracers (other than rhodamine B) were chosen because according to literature data, their absorption and fluorescence spectra only slightly overlap, which minimizes or even avoids the fluorescence self-absorption effect in cases where high tracer concentrations are used or a considerable liquid layer thickness exists between the location of fluorescence excitation and the detector. For rhodamine B and coumarin 152, this effect is investigated in more detail in Sect. 4.4.

3.2 Imaging experiments

For the temperature imaging measurements the beam of a frequency-quadrupled Nd:YAG laser (B.M. Industries, Serie 5000, 266 nm) was formed into a vertical light sheet with a cylindrical telescope (LaVision) resulting in low fluence (1.25×10^5 W/cm^2) excitation. Fluorescence within an area of 31×43 mm^2 was imaged from the calibration cell (cf., Sect. 3.2.2) or the spray flame (cf., Sect. 3.2.1) with an achromatic lens (Nikon, Nikkor UV, $f=105$ mm, f/4.5) onto an intensified CCD camera (LaVision, NanoStar) with a spatial dispersion of 14.8 pixel/mm (67.6 µm/pixel). The non-linearity of the CCD camera is specified by the manufacturer to less than 1% up to its maximum allowable number of counts per pixel. Furthermore the intensifier was operated in the linear regime in medium range gain regions exposing the CCD to not more than 80% of its maximum counts. Chaze et al. (2016) did a detailed analysis regarding the effect of saturation of the molecular transition excited in the dye molecules on the temperature sensitivity of the tracer. According to their results, our experiments were conducted in the linear LIF regime since for the laser dyes they investigated (including rhodamine B, which has a higher absorption cross-section than coumarin 152) the saturation laser fluence was about 1.2×10^6 W/cm^2, which is one order of magnitude above the fluence we used for our measurements with coumarin 152. Two interference filters (ThorLabs) with center wavelengths of 452 and 605 nm (FWHM: 40 nm each) were placed sequentially in front of the lens, and a series of images (5×300 for the calibration, and $7\times3{,}000$ for the spray measurements) was acquired for averaging and further post processing. The experimental setup is shown in Fig. 1.

3.3 Calibration of LIF measurement setup

To calibrate the two-color LIF-measurement setup depicted in Fig. 1, the same temperature-stabilized quartz

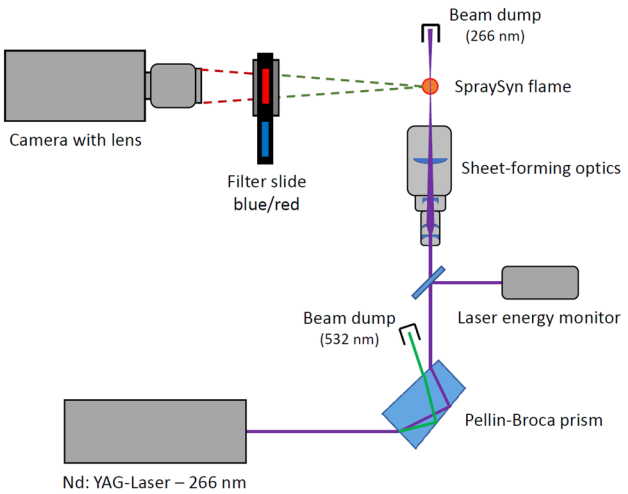

Fig. 1 Two-color laser-induced fluorescence measurement setup for the SpraySyn flame

cuvette utilized in the spectroscopic measurements was placed in the laser sheet at the position of the spray flame (cf., Sect. 3.2.2) and heated to the desired calibration temperature. Calibration measurements were done for various concentrations of coumarin 152 in ethanol. The resulting intensity ratios are presented in Sect. 4.5.

3.4 Liquid-phase temperature measurements in the spray flame

To demonstrate the two-color LIF thermometry with the tracer coumarin 152, a temperature imaging experiment was conducted in an ethanol spray flame generated by the SpraySyn burner designed for the synthesis of metal-oxide nanoparticles (Schneider et al. 2019). In this burner, the liquid exiting from a small capillary (inner/outer diameter: 0.4/0.7 mm) is atomized by a co-annular (internal diameter 1.5 mm) high-speed (approx. 80 m/s at the standard operating condition) dispersion gas flow of oxygen. The spray nozzle is surrounded by a premixed methane/oxygen pilot flame stabilized on a sintered bronze matrix (outer diameter 15 mm). This flame again is shielded against laboratory air by a nitrogen flow through a co-annular 70 mm-diameter sintered bronze matrix. Details of the measurement procedure and the resulting liquid phase temperature field will be shown in Sect. 4.6.

4 Results

4.1 Temperature-dependent fluorescence spectra of coumarin 152 and rhodamine B

In this chapter, the fluorescence spectra of coumarin 152 and rhodamine B dissolved in ethanol are presented for temperatures between 296 and 348 K. Similar data for the other tracers investigated in this work are available in the Supplemental Material. In all the following graphs, the temperature dependence of the fluorescence spectra is depicted in the upper graphs on an individual absolute intensity scale [in counts per second (CPS) as delivered by the spectrometer software] and in the lower graphs as peak-normalized spectra to better illustrate the temperature-dependent variation within the spectral signatures. The temperature-sensitivity factors β (Eq. 1) calculated for a temperature difference of 40 K (between spectra taken at 303 and 343 K) and the positions and spectral widths of optimized (cf. Sect. 4.2 for the optimization constraints) detection bands for calculating the two-color LIF ratios are also plotted in each upper graph of the respective figures.

Coumarin 152 (Fig. 2): Among the Nd:YAG laser harmonics, this tracer can be excited at 266 nm and 355 nm and its fluorescence peaks at around 510 nm at room temperature. The fluorescence spectra range from 430 to 750 nm. At the peak wavelength the absolute fluorescence intensity decreases from 296 to 348 K by about 29%.

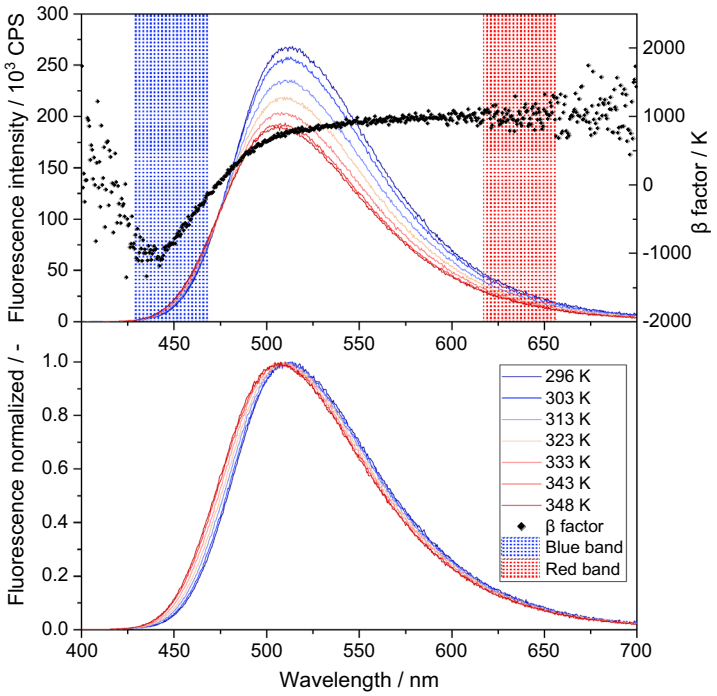

Fig. 2 Upper graph: temperature-dependent fluorescence spectra of coumarin 152 in ethanol (5 mg/l, 1.94×10^{-5} mol/l), excited at 355 nm. Black dots: β factor (evaluated for spectra at 303 and 343 K), colored areas: best compromise for blue and red color-band for thermometry. Lower graph: peak-normalized fluorescence spectra

At wavelengths shorter than 475 nm, the fluorescence intensity increases with temperature whereas at wavelengths larger than 475 nm the intensity decreases. This is reflected in β changing from negative to positive values, which results in a difference of the temperature sensitivity of about 2000 K between the spectral ranges at 445 nm and 640 nm. The normalized fluorescence spectra (Fig. 2, lower graph) exhibit a significant blue shift with temperature (up to 0.15 nm/K in the investigated temperature range).

Rhodamine B (Fig. 3): this tracer has been widely used in the literature for two-color LIF thermometry of liquids with excitation at 514 nm generated by an argon-ion laser (Lavieille et al. 2001). In contrast to excitation at 532 nm (with the blue band as selected here), the former allows the selection of a spectral detection region between 520 and 540 nm, which shows a lower temperature dependence and thus results in a higher temperature sensitivity of the two-color LIF ratio. The spectra of rhodamine B are in good agreement with data presented in Lavieille et al. (2001). For rhodamine B, the use of Nd:YAG lasers is therefore resulting in lower temperature sensitivity compared to the initial demonstration with Ar-ion lasers.

The fluorescence spectra of rhodamine B range from the excitation wavelength of 532–700 nm and their intensities decrease with temperature by a factor of about three in the investigated temperature range. At wavelengths shorter than 590 nm, the peak-normalized spectra show a blue shift (up to 0.1 nm/K). β increases from about 500 K at the blue edge

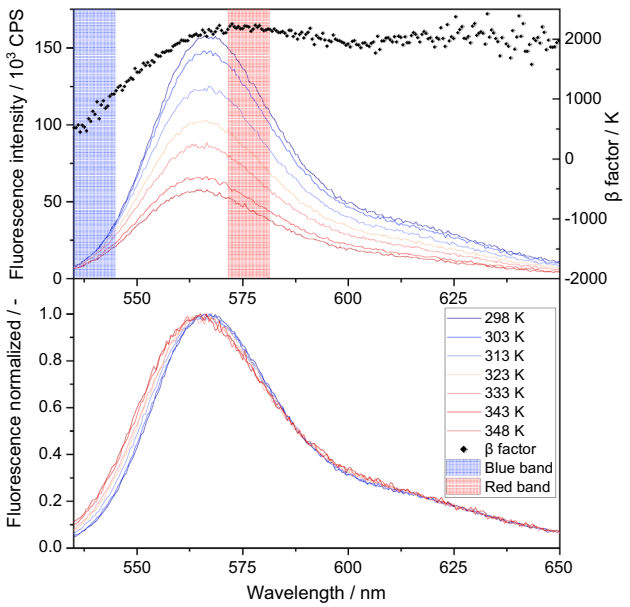

Fig. 3 Upper graph: temperature-dependent fluorescence spectra of rhodamine B in ethanol (0.1 mg/l, 2.1×10^{-7} mol/l), excited at 532 nm. Black dots: β factor (evaluated for spectra at 303 and 343 K), colored areas: best compromise for blue and red color-band for thermometry. Lower graph: peak-normalized fluorescence spectra

of the spectrum to more than 2000 K for wavelengths larger than 570 nm which results in a temperature sensitivity difference of about 1500 K.

Details of the temperature-dependent fluorescence spectra of the other tracers investigated in this work and their β factors are presented in the supplemental material. Contrary to coumarin 152, the intensity of the fluorescence of coumarin 153 only marginally changes with temperature. The temperature sensitivity of the fluorescence (i.e., β) of stilbene 3 is close to zero over most of the spectral range with significant intensity and drops close to $\beta = -3000$ K near its blue edge shorter than 400 nm. The spectra of pyrromethene 597 are fairly self-preserving with temperature with a total intensity drop by a factor of 2.7. β varies non-monotonously between 2100 and 1200 K in the spectral range with significant intensity. The self-preserving spectral shape of pyridine 1 is even more pronounced with a total intensity drop by a factor of 3.1 and no significant peak shift, while β shows a broad and flat maximum around 2000 K.

4.2 Temperature sensitivity for two-color LIF thermometry

To evaluate the suitability of the various tracers for two-color LIF thermometry, a systematic screening of all possible spectral intensity ratios was performed by a Matlab© R2019b software routine using the measured fluorescence spectra. After the band width of the two spectral color bands was manually selected (in this investigation they were fixed to 10 and 40 nm), the code calculates the color-band intensity ratios for all possible combinations of band positions (in increments of 0.5 nm) conditioned to the constraint that the integrated fluorescence intensity within each band exceeds 10% (an arbitrarily fixed value in the measured fluorescence spectra) of the peak intensity (integrated within a 10-nm band). The band positions resulting in the highest temperature sensitivity of the intensity ratio are summarized in Table 2.

It can be generally stated that for the tracers investigated here, the smaller the spectral band width in the detection channels and the lower the intensity constraints, the higher is the attainable temperature sensitivity. However, both trends decrease the signal-to-noise ratio and therefore the applicability needs to be determined beforehand in the respective application to prevent data deterioration because of too weak signals.

To illustrate the evolution of the temperature sensitivities of rhodamine B and coumarin 152 investigated here in more detail, Fig. 4 presents for each tracer in the left column false-color plots of the change of the fluorescence intensity ratio, ΔR_{LIF}, in percent per Kelvin temperature variation, against the respective center-wavelength positions for detection-channel filter bandwidths of 40 nm (coumarin 152, Fig. 4a)

Table 2 Optimized detection bands for two-color LIF thermometry

Tracer	Concentration/(mg/l)	Exc. wavelength/nm	Peak/nm	Band width: 40 nm			Band width: 10 nm		
				Blue band/nm	Red band/nm	Ratio change/(%/K)	Blue band/nm	Red band/nm	Ratio change/(%/K)
Coumarin 152	5	355	509.5	448.5	637.5	1.09	452	620	1.22
Coumarin 153	10	266	531	471.5	660	1.11	475.5	654.5	1.28
DCM	10	266	619.5	545	663.5	0.95	548	661.5	1.07
Pyridine 1	10	532	681	597.5	686	0.49	600	684	0.55
Pyrromethene 597	1	532	567	559	680	0.53	559.5	681.5	0.58
p-Terphenyl	10	266	336	300	354.5	0.21	309	338.5	0.59
Rhodamine 101	6.4	532	598	575.5	681	0.40	567.5	598	0.55
Rhodamine B	0.1	532	566	555	582.5	0.24	540	576.5	1.01
Stilbene 3	10	355	421	375	442	0.51	380.5	428	1.01

Underlying conditions of concentration, excitation wavelength, determined peak position of the fluorescence spectra, central wavelengths and the resulting best spectral band position combinations are given. The resulting temperature sensitivity is given as the relative change of the signal ratio per Kelvin in the temperature range from 303 to 343 K

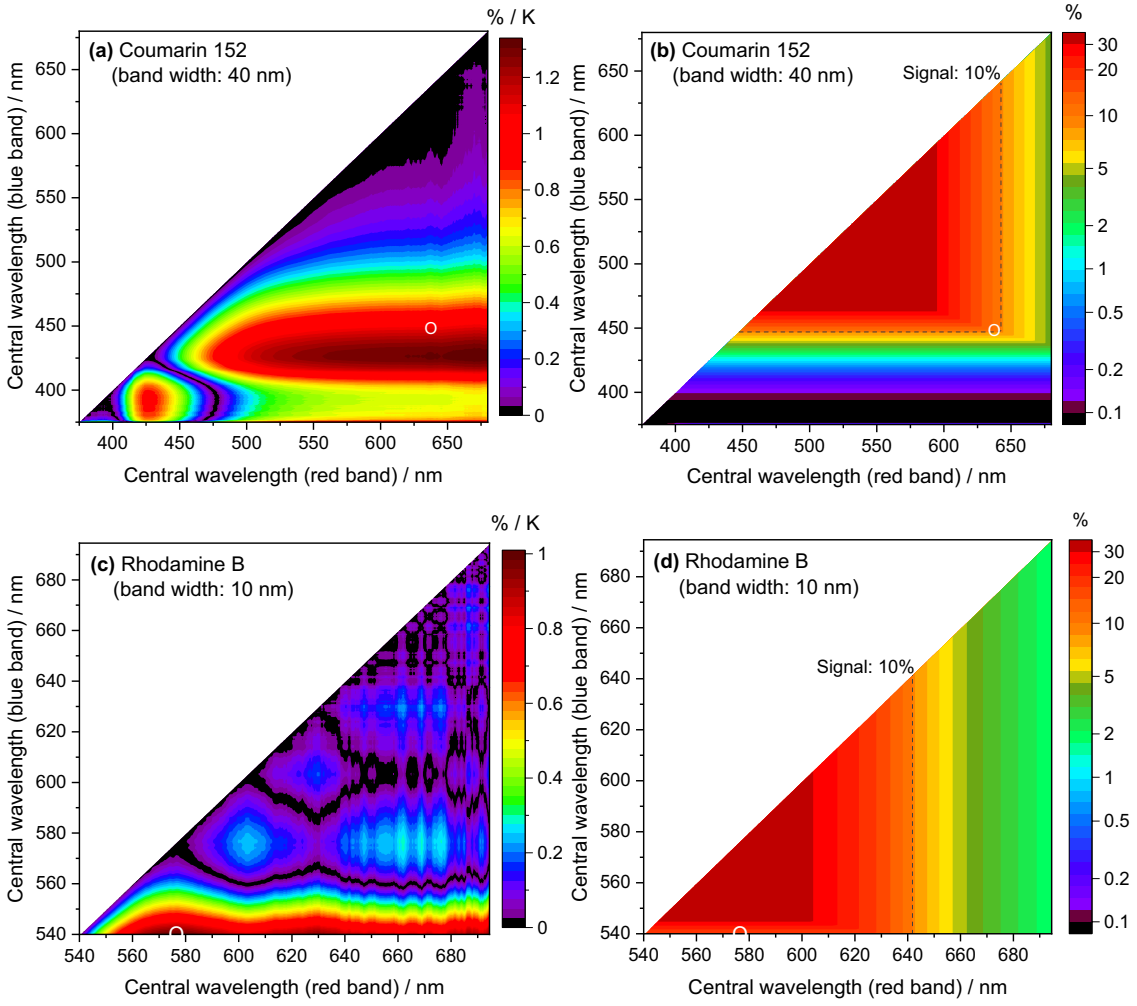

Fig. 4 Left: temperature sensitivity as ratio change in %/K. Right: signal intensity as percentage of peak signal intensity of the weaker channel, **a**, **b**: Coumarin 152, **c**, **d**: Rhodamine B

and 10 nm (rhodamine B, Fig. 4c). To simultaneously estimate the feasibility of a practical temperature measurement, the right column in Fig. 4 depicts (in an exponential false-color scale) the respective fluorescence intensities recorded in the weaker detection channel, which in a more detailed investigation, i.e., considering intensity and detector noise contributing to the measured signal intensities, is an indication of the attainable overall measurement precision. The white circles in each plot mark the selected band positions for the sensitivity optimization of the two-color-LIF intensity ratio plots depicted in Fig. 5. In this context, the dashed lines in the right column plots in Fig. 4b, d mark the 10%-constraint in the detection channel intensities for the two-color intensity-ratio optimization procedure of Fig. 5. As already seen in Fig. 5 the temperature sensitivity in the two-color LIF-ratio method is higher for coumarin 152 than for rhodamine B. It is also noteworthy that for rhodamine B with excitation at 532 nm the blue detection channel cannot access the region of higher sensitivity at shorter wavelengths—contrary to what was achieved by Lavieille et al. with excitation at 514 nm (Lavieille et al. 2001).

The calculated highest intensity ratios (normalized at a reference temperature, $T_0 = 303$ K) for a selection of investigated tracers are presented in Fig. 5. According to the normalized logarithmic ratios plotted against the difference of inverse temperatures the graphs should result in linear dependencies, whose slope is the difference of β between the selected color channels.

Under the above-mentioned experimental conditions and spectral detection constraints it can be derived from the diagrams for both spectral band widths that in case of excitation at Nd:YAG laser harmonics coumarin 152 and coumarin 153 have the highest temperature sensitivity among the investigated tracers. Because of its narrow fluorescence spectra rhodamine B shows a significantly higher temperature sensitivity for a spectral band width of 10 nm than for 40 nm. As known from the literature, higher temperature sensitivities are attainable for rhodamine B in case of excitation at wavelengths shorter than 532 nm because the mostly temperature-independent spectral region located at 520–540 nm becomes accesible (Lavieille et al. 2001). Since a pulsed Nd:YAG laser is preferrable for future single-shot two-color LIF measurements, the tracer coumarin 152 and corresponding filters with a FWHM of 40 nm will be utilised in Sect. 4.6 for temperature imaging in the SpraySyn flame. The approach to calibrate the corresponding ratio-temperature function for this filter set and the measurement setup used is described in more detail in Sect. 4.5.

4.3 Spectral overlap of temperature-dependent absorption and fluorescence spectra of coumarin 152 and rhodamine B

In applications of two-color LIF thermometry where the fluorescence radiation travels through sizeable path lengths of tracer-doped liquid, or where high dye concentrations exist, self-absorption of parts of the LIF signal on its way to the detector, potentially followed by secondary fluorescence emission, affects the two-color LIF signal ratio (Lavieille et al. 2004). Therefore, two of the studied tracers that exhibit a large (coumarin 152) and a small (rhodamine B) Stokes shift were investigated in more detail.

Figure 6 displays the absorption and fluorescence spectra of coumarin 152 at various temperatures. It can be observed that the overlap region of both spectra between 430 and 470 nm is comparatively small with respect to the spectral integral. The absorption cross-section does not change significantly with temperature, and is almost equal to each other at the two standard Nd:YAG laser excitation wavelengths of 266 nm (not shown) and 355 nm; at the

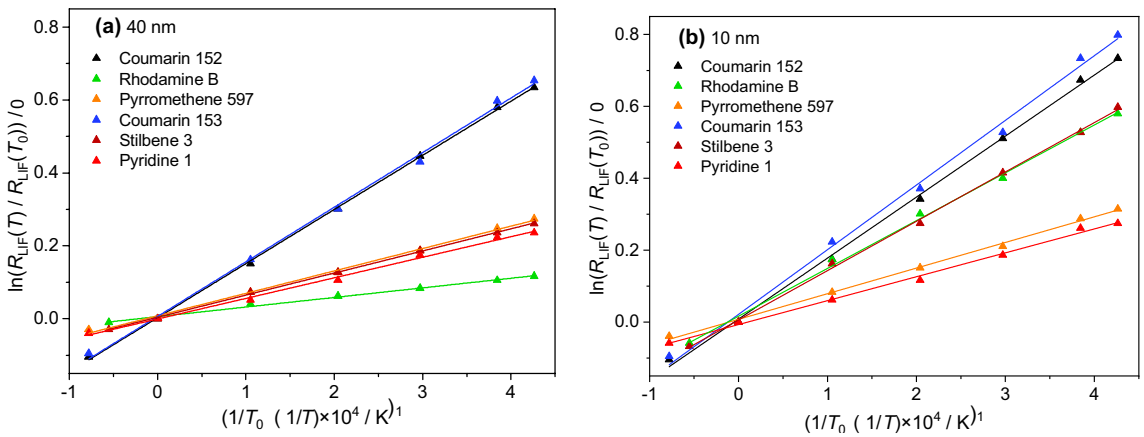

Fig. 5 Calculated fluorescence intensity ratios (symbols) for selected tracers dissolved in ethanol based on measured spectra normalized at 303 K, solid lines: linear fit of intensity ratios, assumed spectral band widths: **a** 40 nm **b** 10 nm

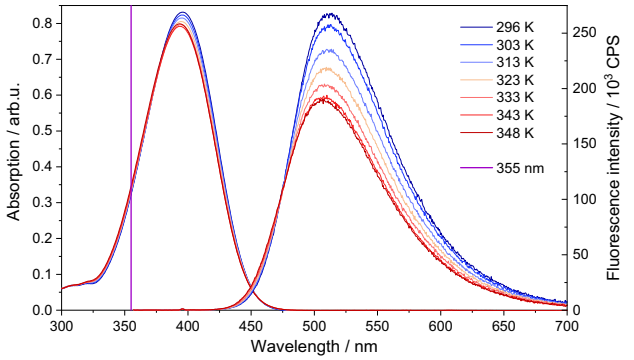

Fig. 6 Temperature-dependent absorption (left) and fluorescence (right) spectra of coumarin 152 in ethanol (5 mg/l, 1.94×10^{-5} mol/l). The vertical line indicates the Nd:YAG excitation wavelength of 355 nm

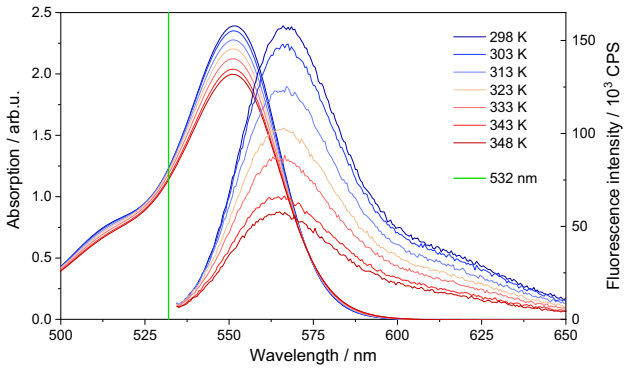

Fig. 7 Temperature-dependent absorption (left) and fluorescence (right) spectra of rhodamine B in ethanol (0.1 mg/l, 2.1×10^{-7} mol/l). The vertical line indicates the Nd:YAG excitation wavelength of 532 nm

excitation wavelength of 266 nm used in this work the absorption cross section varies by 0.9% (0.017%/K) in the considered temperature range.

Contrary to coumarin 152, the Stokes shift of rhodamine B is much smaller (Fig. 7), causing a significant fraction of the spectra to overlap in the region below 590 nm, which in the mentioned cases will lead to partial signal attenuation (cf., Sect. 4.4) and secondary fluorescence emission affecting the detected signal intensity ratios. This effect necessitates corrections of the two-color LIF-thermometry method, e.g., by introducing a three-color ratio technique (Lavieille et al. 2004). Figure 7 also indicates that there is a 7.6% (0.152%/K) variation of the absorption cross-section at the Nd:YAG excitation wavelength of 532 nm in the considered temperature range.

4.4 Concentration dependence of the fluorescence spectra of rhodamine B and coumarin 152

From the previous section it is clear that the absorption and fluorescence spectra of rhodamine B overlap significantly (Lavieille et al. 2001), whereas for coumarin 152 this is much less the case. Signal self-absorption was already described for rhodamine B by Lavieille et al. (2004) who were able to correct this drawback with a three-color detection technique by forming signal ratios between LIF intensities measured in a temperature-insensitive channel and in two temperature-sensitive channels with and without suffering fluorescence signal trapping, respectively.

To investigate the impact of self-absorption for the spectra of coumarin 152 and rhodamine B, fluorescence spectra were recorded in 10×10 mm^2 cuvettes, where the optical path length of fluorescence light through the tracer-doped liquid is about 5 mm in the standard 90° excitation/detection geometry. Additionally, fluorescence measurements were done under the same conditions using thin-layer cuvettes in a front-illuminating geometry (a 22.5° angle between excitation and detection light paths) providing path lengths of 50 and 100 µm depending on cuvette thickness. This latter situation is similar to the spray measurements described in Sects. 3.2.2 and 4.6 with small and sparse droplets in the measurement volume.

The fluorescence spectra for the two measurement configurations are presented in Fig. 8 for concentrations starting at 0.5 mg/l (coumarin 152) and 0.1 mg/l (rhodamine B), spanning a factor of 100. All spectra were measured at 303 K and are plotted for the 5-mm absorption path-length and the thin-layer cuvettes with solid and dashed lines, respectively. The spectra are normalized at a wavelength where no overlap exists with the absorption spectra (i.e., 600 and 630 nm for coumarin 152 and rhodamine B, respectively). For comparison, the respective absorption spectra in the spectral overlap region of interest are plotted on a separate *y*-axis. The spectra illustrate the effect of fluorescence self-absorption in the spectral regions where significant overlap with the absorption spectrum exists. Due to its large Stokes shift, the spectrum of coumarin 152 is largely unaffected, while for rhodamine B there is an apparent spectral shift and attenuation of the peak, depending on the concentration and/or re-absorption path length through the sample.

Even for small optical path lengths like 100 µm, a reduction of the detected fluorescence intensity and a red shift of the spectra of rhodamine B can be observed, whereas for coumarin 152 this is not measurable. It can be concluded that for the two-color LIF thermometry method with considerable absorption path lengths or comparatively high tracer concentrations, coumarin 152 with its large Stokes shift significantly reduces the measurement error caused by self-absorption effects.

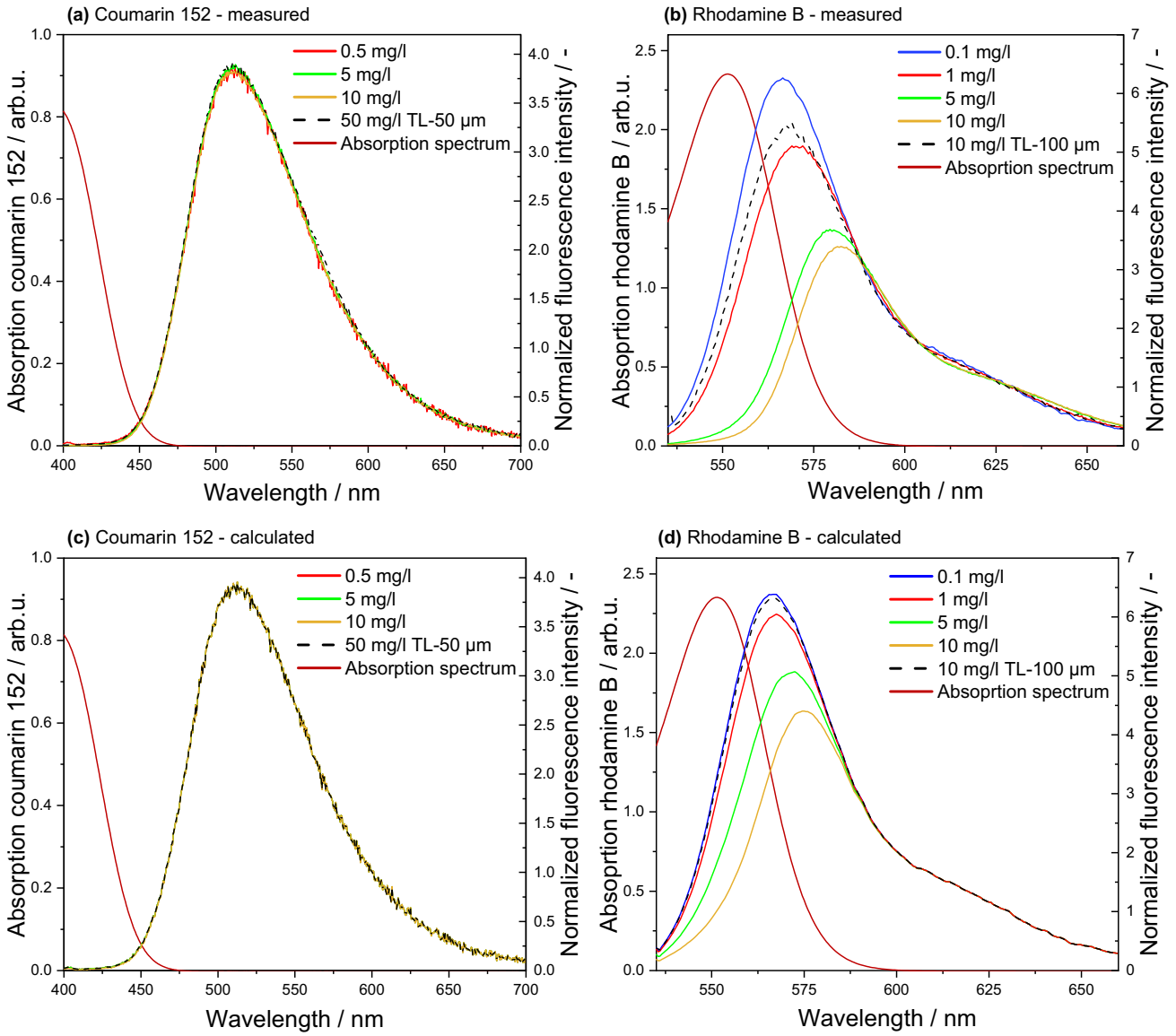

Fig. 8 Top: Measured fluorescence spectra of coumarin 152 (**a**) and rhodamine B (**b**) for samples at various concentrations and reabsorption path lengths (5 mm within a 10×10 mm^2 cuvette (solid lines), or a thin layer cuvette [50 µm (**a**, **c**), or 100 µm (**b**, **d**), (dashed lines)] at 303 K: the spectra are normalized at 600 nm (**a**, **c**) and at 630 nm (**b**, **d**), respectively. Bottom: calculated fluorescence spectra of coumarin 152 (**c**) and rhodamine B (**d**) using a simple reabsorption model (see text)

The measured results agree reasonably well with a simple model calculation of self-absorption-affected fluorescence spectra. This is illustrated by the lower row of graphs in Fig. 8, which shows spectra scaled according to the reabsorption effects at the same concentrations and absorption path lengths as given in the experiments. The calculations were done under the simplifying assumptions that the fluorescence signal linearly scales with dye concentration (ignoring quenching effects) and that the excitation light intensity at the probe volume is the same for all concentrations. The fluorescence spectra generated in solutions with higher tracer concentrations were calculated from the measured low-concentration spectra using the Beer-Lambert law

$$I = I_0 \exp\left(-\varepsilon_\lambda c d\right), \tag{5}$$

with transmitted light I, incident light I_0, the molar attenuation coefficient ε_λ, the dye concentration c and the assumed absorption path length d, through the liquid towards the detector. The molar attenuation coefficient ε_λ was measured for coumarin 152 at 396 nm with 2.1×10^4 l/(mol cm) and for rhodamine B at 552 nm with 11.2×10^4 l/(mol cm) which is very close to the values given by Brackmann (2000). The

results of this simple model are presented in the lower row of Fig. 8 [for coumarin 152 (c) and rhodamine B (d)]. It can be observed that for rhodamine B the measured peak reduction and the resulting apparent peak shift in the measured fluorescence spectra is larger than suggested by the calculated results, whereas for coumarin 152 the spectra are virtually unaffected by re-absorption effects.

Overall, since this simplified model confirms the trends observed in the experiments in the investigated concentration range, the calculations prove that the change of the fluorescence spectra is mainly driven by self-absorption, and not caused by tracer–tracer interactions. Due to the increased re-absorption of fluorescence radiation in the blue wing of the rhodamine B spectra, the normalized fluorescence peak is shifted to longer wavelengths, which will predominantly affect the "blue" fluorescence channel—and thus the fluorescence ratio used for the two-color thermometry. The results also suggest that, because this effect is negligible for coumarin 152, it makes this tracer a promising candidate for temperature measurements in spatially extended evaporating sprays with variation in concentration or in tracer-doped fluids in large-scale containers with significant re-absorption path lengths.

4.5 Calibration of the signal-ratio-temperature function

As described in Sect. 3.2.1, the two-color imaging setup was calibrated with homogeneous ethanol/coumarin 152 solutions for a range of temperatures and various concentrations in a temperature-stabilized quartz cuvette. The two-color LIF ratios were determined for temperatures between 296 and 348 K by taking 300 fluorescence images of the cuvette through the chosen filters. In the following Matlab evaluation code the fluorescence images were background and laser-pulse-energy corrected to compensate background light and laser intensity fluctuation. In the next step the corrected fluorescence intensity from a region of interest was averaged and the ratios were calculated from the respective LIF-signal ratio at various solution temperatures. The resulting intensity ratios are plotted versus temperature and are shown for three solute concentrations in the diagram in Fig. 9.

The temperature dependence of the two-color intensity ratio follows the expected behavior based on the measured fluorescence spectra (Fig. 9). Due to the large Stokes shift in case of coumarin 152, the ratio function does not change within the tracer concentration range investigated here. A least-squares data fit with an exponential function ($R^2 = 0.99786$) results in

$$T\left(R_{\mathrm{LIF}}\right) = 383.39184 - 197.74433 \exp\left(-0.981\, R_{\mathrm{LIF}}\right). \quad (6)$$

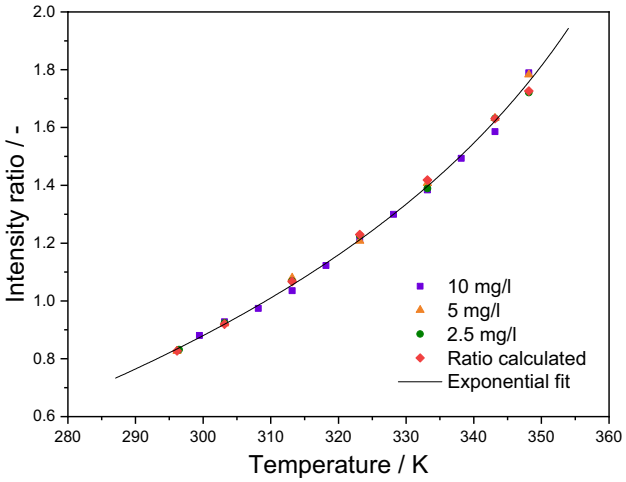

Fig. 9 Two-color LIF intensity ratios (symbols) as a function of temperature, measured for coumarin 152 solutions (2.5, 5, 10 mg/l in ethanol). An exponential fit is plotted as solid line. Intensity ratios calculated from the measured spectra (5 mg/l solution) are shown as red diamonds

To compare the calibration results to the optimal ratio-temperature function derived from the measured fluorescence spectra, the calculated ratios are normalized to the fit function at 303 K and plotted to Fig. 9. The accordance of the calibrated to the calculated ratio-temperature function is very high. In the following the determined signal-ratio-temperature function is used to convert measured ratios to their corresponding temperature.

4.6 Temperature imaging in an ethanol spray flame

The temperature imaging capability of coumarin 152 is demonstrated in an ethanol spray flame generated by the SpraySyn burner (Schneider et al. 2019). The liquid fuel was seeded with 10 mg/l coumarin 152 and excited by the 266-nm laser sheet. The resulting fluorescence was detected sequentially through the blue and red filter as described in Sect. 3.2.2. Because the spray is sparse, a large number of individual experiments were averaged [21,000 LIF images and 4200 background images (without laser excitation) in sequences of 3000 LIF images and 600 background images each] to generate a continuous intensity distribution for each color channel. The background-subtracted LIF images were corrected for fluctuations in laser intensity using the data from the reference photodiode before averaging and are depicted in Fig. 10 for the red (a) and blue (b) channel with an exponential color scale. In the last step, both LIF signal maps are divided pixel by pixel to obtain the ratio map that was finally converted by the determined signal-ratio-temperature function (Fig. 9) to the desired temperature map shown in Fig. 10c). For

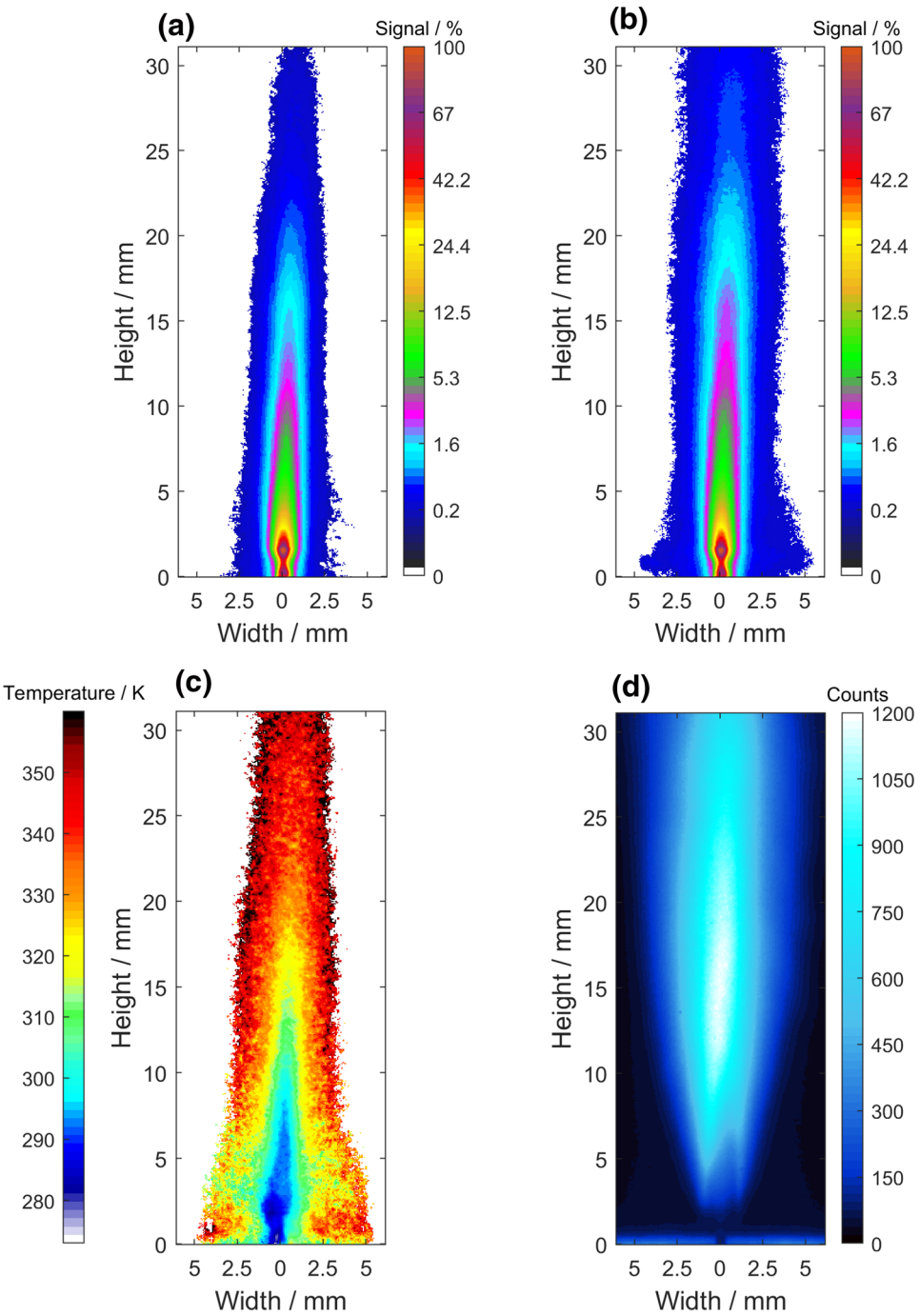

Fig. 10 SpraySyn flame operated with ethanol seeded with coumarin 152 (10 mg/l, 3.89×10^{-5} mol/l). Burner operating conditions: 5 ml/min ethanol, 10 slm O_2 dispersion gas, 2/16 slm CH_4/O_2 pilot flame, 120 slm N_2 coflow, **a** red and **b** blue LIF channel (exponential color scale). **c** Liquid-phase temperature map. **d** Flame luminescence intensity map in false colors

comparison with the visible flame structure within the same field of view, the intensity of the flame luminescence (measured without any optical filters in front of the camera) is shown in Fig. 10d) as a false color image.

For the depiction of the temperature map pixels with signal levels in either one of the color channels below a LIF-signal threshold of 0.5 counts in average per image were colored white (maximum values of averaged counts per pixel are ranging in the magnitude of 500 counts). It is expected that after droplet evaporation the tracer disintegrates and oxidizes with no significant fluorescence generated from the gas phase.

The SpraySyn flame features a highly turbulent combustion process for which "true" temperatures would only be obtained with optical diagnostics of instantaneous (i.e., single-pulse) measurement capability. For the current method this would need simultaneous image acquisition of the two color channels, e.g., by two separate cameras triggered simultaneously. Therefore, with the current measurement strategy only temporally averaged temperature

fields can be obtained. An error propagation analysis was conducted to estimate the uncertainty of the present approach. The analysis included the magnitude of the camera noise and the fluctuation of the measured ratio to quantify the statistical error (ranging in the magnitude of $\Delta R/R = 0.1–0.4\%$), the standard error of the fit parameters of Eq. (6) calculated by least-square fitting ($\Delta a/a = 1.19\%$, $\Delta b/b = 1.93\%$, $\Delta c/c = 8\%$), and the uncertainty of the thermocouple measurements ($\Delta T = \pm 0.15$ K). A Matlab routine was created to calculate the uncertainty of the measured temperature for every single pixel resulting in values ranging from 6.5 to 9.5 K depending on the region within the liquid-phase temperature map. The measurement uncertainty in the outer regions of the flame shows higher values due to the strong intermittency of the signal compared to regions close to the capillary outlet where LIF signal is detected regularly. For validation purposes the temperature in the spray core of liquid ethanol at the capillary outlet without flame was measured by a thermocouple showing values down to less than 278 K due to ethanol evaporation. Consequently, the measured temperatures at the capillary outlet at around 283 K are considered consistent.

5 Conclusions

In this work, two-color LIF thermometry using coumarin 152 as tracer is introduced. Due to a large Stokes shift, this approach is less affected by self-absorption than comparable temperature tracers used in the literature. Consequently, this method is especially suitable for sprays or droplets facing evaporation, which causes changes in concentration and thus signal self-absorption. Additional corrections for self-absorption as suggested in previous publications with using a third detection channel become unnecessary resulting in a simplified experiment with two detection channels only. Coumarin 152 can be excited with pulsed Nd:YAG lasers (at 266 or 355 nm) and provides a high-temperature sensitivity. Comparisons to the tracer rhodamine B that is widely used for two-color LIF were carried out and pros and cons determined. To prove the new approach, the two-color LIF thermometry with coumarin 152 was demonstrated by measuring the liquid-phase temperature map of an ethanol spray flame with 266-nm excitation. Due to a high fluorescence quantum yield it was possible to conduct these measurements with a very low tracer concentration of 10 mg/l (3.89×10^{-5} mol/l).

Acknowledgements Financial support by the German Research Foundation (DFG) within PP 1980 "Nanoparticle synthesis in spray flames" under contract 374463258 is gratefully acknowledged.

References

Angel S, Neises J, Dreyer M, Friedel-Ortega K, Behrens M, Wang Y, Arandiyan H, Schulz C, Wiggers H (2019) Spray-flame synthesis of the nanosized La(Fe, Co)O_3 nano-perovskites from metal nitrates. AIChE J 66:e16748. https://doi.org/10.1002/aic.16748

Berrocal E, Kristensson E, Richter M, Linne M, Alden M (2008) Application of structured illumination for multiple scattering suppression in planar laser imaging of dense sprays. Opt Express 16:17870–17881. https://doi.org/10.1364/oe.16.017870

Brackmann U (2000) Lambdachrome laser dyes. Lambda Physik AG, Göttingen

Chaze W, Caballina O, Castanet G, Lemoine F (2016) The saturation of the fluorescence and its consequences for laser-induced fluorescence thermometry in liquid flows. Exp Fluids 57:58. https://doi.org/10.1007/s00348-016-2142-8

Copetta J, Rogers C (1998) Dual emission laser induced fluorescence for direct planar scalar behavior measurements. Exp Fluids 25:1–15

Deprédurand V, Miron P, Labergue A, Wolff M, Castanet G, Lemoine F (2008) A temperature-sensitive tracer suitable for two-colour laser-induced fluorescence thermometry applied to evaporating fuel droplets. Meas Sci Technol 19:105403–105412. https://doi.org/10.1088/0957-0233/19/10/105403

Duwel I, Koban W, Zimmermann FP, Dreier T, Schulz C (2009) Spectroscopic characterization of the fluorobenzene/DEMA tracer system for laser-induced exciplex fluorescence for the quantitative study of evaporating fuel sprays. Appl Phys B Lasers O 97:909–918. https://doi.org/10.1007/s00340-009-3652-3

Greszik D, Yang H, Dreier T, Schulz C (2011) Laser-based diagnostics for the measurement of liquid water film thickness. Appl Opt 50:A60–67. https://doi.org/10.1364/AO.50.000A60

Heinisch C, Wills JB, Reid JP, Tschudi T, Tropea C (2009) Temperature measurement of single evaporating water droplets in a nitrogen flow using spontaneous Raman scattering. Phys Chem Chem Phys 11:9720–9728. https://doi.org/10.1039/b908555f

Horn J, Chigier N (2002) Rainbow refractometry: simultaneous measurement of temperature, refractive index, and size of droplets. Appl Opt 41:1899–1907

Lavieille P, Lemoine F, Lavergne G, Virepinte JF, Lebouché M (2000) Temperature measurements on droplets in monodisperse stream using laser-induced fluoresence. Exp Fluids 29:429–437

Lavieille P, Lemoine F, Lavergne G, Lebouche M (2001) Evaporating and combusting droplet temperature measurements using two-color laser-induced fluorescence. Exp Fluids 31:45–55. https://doi.org/10.1007/s003480000257

Lavieille P, Delconte A, Blondel D, Lebouche M, Lemoine F (2004) Non-intrusive temperature measurements using three-color laser-induced fluorescence. Exp Fluids 36:706–716. https://doi.org/10.1007/s00348-003-0748-0

Lefebvre AH, McDonell VG (2017) Atomization and sprays. Combustion: an international series. CRC Press, Boca Raton

Melton LA (1993) Exciplex-based vapor liquid visualization systems appropriate for automotive gasolines. Appl Spectrosc 47:782–786. https://doi.org/10.1366/0003702934067081

Mishra YN, Abou Nada F, Polster S, Kristensson E, Berrocal E (2016) Thermometry in aqueous solutions and sprays using two-color LIF and structured illumination. Opt Express 24:4949–4963. https://doi.org/10.1364/OE.24.004949

Muller T, Grunefeld G, Beushausen V (2000) High-precision measurement of the temperature of methanol and ethanol droplets using spontaneous Raman scattering. Appl Phys B Lasers O 70:155–158. https://doi.org/10.1007/s003400050024

Murray AM, Melton LA (1985) Fluorescence methods for determination of temperature in fuel sprays. Appl Opt 24:2783–2787. https://doi.org/10.1364/ao.24.002783

Raffius T, Schulz C, Ottenwalder T, Grunefeld G, Koss HJ, Brands T, Pischinger S (2017) Flame-temperature, light-attenuation, and CO measurements by spontaneous Raman scattering in non-sooting diesel-like jets. Combust Flame 176:104–116. https://doi.org/10.1016/j.combustflame.2016.09.027

Rosebrock CD, Wriedt T, Madler L, Wegner K (2016) The role of microexplosions in flame spray synthesis for homogeneous nanopowders from low-cost metal precursors. AiChE J 62:381–391. https://doi.org/10.1002/aic.15056

Roth N, Anders K, Frohn A (1991) Refractive-index measurements for the correction of particle sizing methods. Appl Opt 30:4960–4965. https://doi.org/10.1364/AO.30.004960

Schaschek K, Popp J, Kiefer W (1993) Observation of morphology-dependent input and output resonances in time-dependent raman-spectra of optically levitated microdroplets. J Raman Spectrosc 24:69–75. https://doi.org/10.1002/jrs.1250240203

Schneider F, Suleiman S, Menser J, Borukhovich E, Wlokas I, Kempf A, Wiggers H, Schulz C (2019) SpraySyn-A standardized burner configuration for nanoparticle synthesis in spray flames. Rev Sci Instrum 90:085108. https://doi.org/10.1063/1.5090232

Schulz C, Sick V (2005) Tracer-LIF diagnostics: quantitative measurement of fuel concentration, temperature and fuel/air ratio in practical combustion systems. Prog Energy Combust Sci 31:75–121. https://doi.org/10.1016/j.pecs.2004.08.002

Snow JB, Qian SX, Chang RK (1985) Stimulated Raman-scattering from individual water and ethanol droplets at morphology-dependent resonances. Opt Lett 10:37–39. https://doi.org/10.1364/Ol.10.000037

Tropea C, Yarin AL, Foss JF (2007) Handbook of experimental fluid mechanics. Springer, Berlin

Walrafen GE, Fisher MR, Hokmabadi MS, Yang W-H (1998) Temperature dependence of the low- and high-frequency Raman scattering from liquid water. J Chem Phys 85:6970–6982

Wang CH, Fu SY, Kung LJ, Law CK (2005) Combustion and microexplosion of collision-merged methanol/alkane droplets. Proc Combust Inst 30:1965–1972. https://doi.org/10.1016/j.proci.2004.08.111

Wieske P, Wissel S, Grunefeld G, Pischinger S (2006) Improvement of LIEF by wavelength-resolved acquisition of multiple images using a single CCD detector—simultaneous 2D measurement of air/fuel ratio, temperature distribution of the liquid phase and qualitative distribution of the liquid phase with the Multi-2D technique. Appl Phys B Lasers O 83:323–329. https://doi.org/10.1007/s00340-006-2173-6

Yang H, Greszik D, Wlokas I, Dreier T, Schulz C (2011) Tunable diode laser absorption sensor for the simultaneous measurement of water film thickness, liquid- and vapor-phase temperature. Appl Phys B Lasers O 104:21–27. https://doi.org/10.1007/s00340-011-4643-8